J Mater Sci (2008) 43:1357–1365
DOI 10.1007/s10853-007-2283-5

Scratch behavior of soft thermoplastic olefins: effects of ethylene content and testing rate

Robert L. Browning · Han Jiang · Allan Moyse · Hung-Jue Sue · Yuki Iseki · Kousuke Ohtani · Yasuhito Ijichi

Received: 25 July 2007 / Accepted: 30 October 2007 / Published online: 12 December 2007

Abstract Soft thermoplastic olefins (TPOs) consisting of 70 wt.% ethylene–propylene rubber (EPR) and 30 wt.% polypropylene (PP) were subjected to a standardized scratch test (ASTM D7027-05) at three different testing speeds: 1, 10, and 100 mm/s. Two TPO systems were considered for the study: System A having 52 wt.% ethylene in the EPR and System B containing 67 wt.% ethylene. Raising the ethylene content in EPR not only increased the overall blend crystallinity, but also altered the internal morphology of the material. Scratch testing rate appears to impart a significant effect on the scratch behavior of the material. The scratch damage mechanisms and morphology in the above model systems are described and correlated with tensile behavior and mechanical properties to establish a structure–property relationship. Issues regarding scratch properties of the soft TPOs are discussed.

Introduction

Thermoplastic olefins (TPOs) offer a wide range of material properties that are attractive to the polymer processing industry. Applications of TPOs have been mainly limited to rigid materials used for structural purposes to replace metal parts and specialty polymers such as automobile bumper fascia and interior/exterior components. Rigid TPOs have been studied extensively and their properties are fairly well understood [1–10]. The automotive industry specifically has enjoyed several benefits from rigid TPOs such as lower production cost, shorter production time, increased safety, improved fuel efficiency, and many others. Given the many advantages mentioned above, TPOs have now been modified to exhibit appropriate softness for expanded automotive and appliance uses.

By adjusting the polypropylene (PP)-to-elastomer ratio, the properties of the material can be drastically altered [11–14]. Automotive-grade rigid TPOs are generally composed of 70 wt.% PP and 30 wt.% elastomer. This ratio provides the material with enough rigidity from the PP phase for structural purposes while having adequate impact resistance from the elastomer phase. In order to achieve a "soft-touch" feel similar to leather, elastomer content in such TPOs is usually greater than 60% by weight. These soft TPOs show promise for a variety of automotive and appliance applications. Due to their high elastomer content, changing the properties of the elastomer can greatly affect both physical and mechanical properties of soft TPOs.

The elastomer ethylene–propylene rubber (EPR) is made by a random copolymerization of ethylene and propylene. Since polyethylene (PE) segments in EPR can crystallize readily, an elastomer with high ethylene content will become more rigid. This means that the hardness of a flexible, elastomer-rich TPO can be tuned not only by the elastomer content, but also by adjusting the ethylene–propylene monomer ratio of the elastomer used.

The tunable hardness nature of these soft TPO materials implies that they can potentially be useful as a low-cost,

R. L. Browning · H. Jiang · A. Moyse · H.-J. Sue (✉)
Polymer Technology Center, Department of Mechanical Engineering, Texas A&M University, College Station, TX 77843-3123, USA
e-mail: hjsue@tamu.edu

Y. Iseki
Sumitomo Chemical America, New York, NY, USA

K. Ohtani · Y. Ijichi
Sumitomo Chemical Company, Chiba, Japan

recyclable alternative to vulcanized rubbers for artificial leather and non-skid surfaces. Cross-linking of these materials could lead to further applications such as the fabrication of low-temperature O-ring seals and gaskets. For automotive applications, these soft materials must have good scratch resistance. The scratch behavior of many rigid polymers has been studied in the past [15–42], but the behavior of soft polymers is still not very well understood. In this work, EPR-rich soft TPOs were used to investigate the effects of ethylene content of the elastomer phase and testing rate on the mechanical properties of the materials with a focus on correlation of tensile properties with their scratch behavior. Scratch damage mechanisms are investigated and issues related to the scratch behavior of soft TPOs will be discussed.

Experimental

Model systems

Compression-molded EPR-rich soft TPO sheets for this study were provided by Sumitomo Chemical, Ltd. in Japan with the compositions shown in Table 1. After compounding, pellets of Systems A and B were molded into 150 mm by 150 mm by 2 mm sheets at 220 °C and 5 MPa with an F-37 compression molder (Shinto Metal Industries, Ltd.). These compression-molded soft TPOs show no signs of surface anisotropy. However, they still exhibit evidence of skin-core morphology, as will be described below.

Thermal and mechanical characterization

All thermal and mechanical characterization was carried out by Sumitomo Chemical. Differential scanning calorimetry (DSC) was carried out using a TA DSC Q100 at a heating rate of 5 °C/min with N_2 purge gas. Shore-A hardness was measured with a durometer in accordance with ASTM D2240. Tensile properties were characterized following ASTM D412 using Die C geometry in an Instron 5565 Extra Height testing apparatus at testing speeds of 0.083, 0.83, and 8.3 mm/s at 23 °C and 50% relative humidity. Static and kinetic coefficients of friction were measured in compliance with JIS K 7125 (analogous to ASTM D1894).

Scratch testing

Scratch testing was performed using the testing apparatus and methodology outlined in ASTM D7027–05 [43] at scratch velocities of 1, 10, and 100 mm/s using a stainless steel ball bearing scratch tip (Diameter = 1 mm).

System A was tested at a load range of 0.5–7 N and a scratch length of 82 mm to prevent penetration of the scratch tip through the material, while a progressive normal load of 0.5–10 N was employed for the more rigid System B with a scratch length of 120 mm. The 82 mm scratch length is scaled from the 120 mm test so that the applied normal loads would correspond to the same rate of load increase during tests.

Post-scratch analysis of scratched samples

After being subjected to the testing conditions described above, the samples were scanned using an EPSON 4870 Perfection Photo flatbed PC scanner at a resolution of 800 dpi in 8-bit grayscale mode. The samples were inherently translucent, so a piece of black paper with a light emission rating of 0.2% was placed behind the samples to introduce contrast between the scratched and undamaged portions of the samples. Additionally, the gray levels were normalized by scanning a black-to-white gradient bar (0–255 in grayscale value; 0 = black, 255 = white) simultaneously with the tested samples. This normalization technique ensured that the image obtained in the scanning software is representative of the actual sample as observed with human eyes.

In a scratch where the applied load is increased as a function of length, transitions in the scratch damage mechanisms can be observed, as will be discussed below. Taking into account that the applied normal load increases linearly with scratch length, the following equation is used to correlate the point at which a transition occurs to the applied normal load at that point:

Table 1 Composition of model soft TPO systems

	System A		System B	
	In bulk (wt.%)	In elastomer (wt.%)	In bulk (wt.%)	In elastomer (wt.%)
EPR Elastomer Content	70	Ethylene 52 Propylene 48	70	Ethylene 67 Propylene 33
PP Content	30	–	30	–

$$F_c = \frac{(L-x)}{L}(F_f - F_0) + F_0 \quad (1)$$

where F_c is the critical load where a transition in damage mechanism occurs (N), L is the total scratch length (mm), x is the distance from the end of the scratch to the feature of interest along the scratch track (mm), and F_f and F_0 are the final and initial applied normal loads (N), respectively.

Scanning electron microscopy observation

Internal morphology of the soft TPOs was observed by Sumitomo Chemical using a Hitachi S-800 SEM. Cross sections of the material were cut with a microtome and then subjected to a treatment with a chromic acid agent that allowed for preferential etching away of the elastomer phase.

A JEOL JSM-6400 SEM operated at an accelerating voltage of 15 kV was employed at Texas A&M University to observe the resulting scratch damage features at a sufficiently high resolution. Ten by 20 mm blocks were cut from specimens of Systems A and B where the point of interest was centered within each block. The blocks were then coated with 400 Å of AuPd to prevent charging.

Scratch depth analysis

A Dektak 3 Stylus Profilometer (Veeco Metrology, Inc.) was used to investigate the rate dependence of the deformation of System A by measuring the scratch depth at points in the scratch corresponding to applied normal loads of 1.6, 2.7, and 3.8 N. The radius of the diamond stylus was 12.5 μm and the normal force applied to the stylus is factory-set to a value of 0.5 μN. The horizontal resolution is controlled by the scan speed and scan length. Analog electronics were equipped to detect and amplify the signal from the transducer.

Results and discussion

Effect of ethylene content in EPR

The DSC curves in Fig. 1 suggest that raising the concentration of ethylene in EPR from 52 wt.% to 67 wt.% not only raises the T_g of the soft TPO, but also increases the crystallinity of the elastomer. As indicated in Fig. 1, System B displays a broad melting peak corresponding to PE in the EPR at ~21 °C while there is no such detectable peak for System A. This observation was verified by performing DSC scans on the individual constituents of

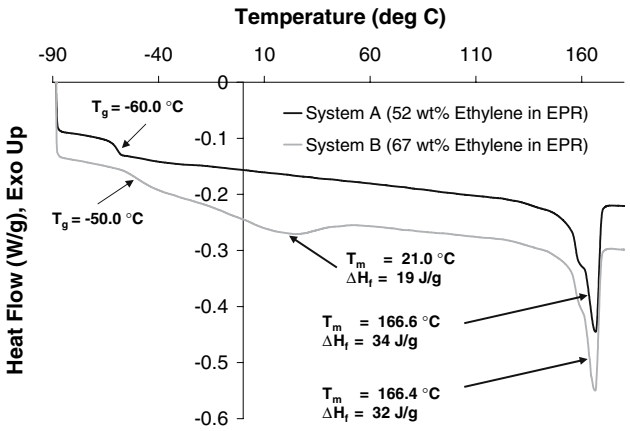

Fig. 1 DSC curves (second heating) for model soft TPO systems

Systems A and B, i.e., both types of elastomer and PP as separate entities (not shown). The curve for the EPR in System B did indeed show a similar peak at ~21 °C corresponding to the PE phase, while no peak was detected within this range for the EPR of System A.

The percentage crystallinity (X) based on weight of EPR in the TPO was found using the following equation:

$$X = \left(\frac{\Delta H_{f,PE}}{\Delta H_{f,PE(X=100\%)}}\right) \cdot \left(\frac{100\text{ g TPO}}{70\text{ g EPR}}\right) \cdot 100\% \quad (2)$$

where $\Delta H_{f,PE}$ is the crystalline melting enthalpy of PE in the EPR obtained from the DSC curve (J/g) and $\Delta H_{f,PE(X=100\%)}$ is the heat of fusion associated with melting a 100% crystalline PE specimen ($\Delta H_{f,PE(X=100\%)} = 290$ J/g) [44]. Using the information from Fig. 1 and plugging into Eq. 2, the EPR of System A is found to be amorphous while that of System B is 9.4 % crystalline.

The DSC curves also show that the peak corresponding to PP melting remains unaffected. Literature provides evidence that addition of EPR to PP neither inhibits nor promotes overall crystallinity of the PP phase [21]. However, it is suggested by several sources that the small shoulder present in the PP peak just before 160 °C on both DSC curves is more than likely due to the presence of β-form PP spherulites [45–47].

The crystallinity of EPR depends on the ethylene content of the elastomer. At low ethylene content, the numerous randomly distributed methyl branches associated with the propylene portions of EPR will disrupt crystallization of the random copolymer. However, as the ethylene content increases, PE segments become dominant in the elastomer, allowing for PE segments to fold upon themselves and form PE crystalline lamellae. The resulting crystalline portions of the elastomer may hinder the interfacial inter-mixing between PP and EPR, thereby resulting in an increase in EPR domain size and poor bonding which could lead to micro-voiding under stress. Figure 2 shows a

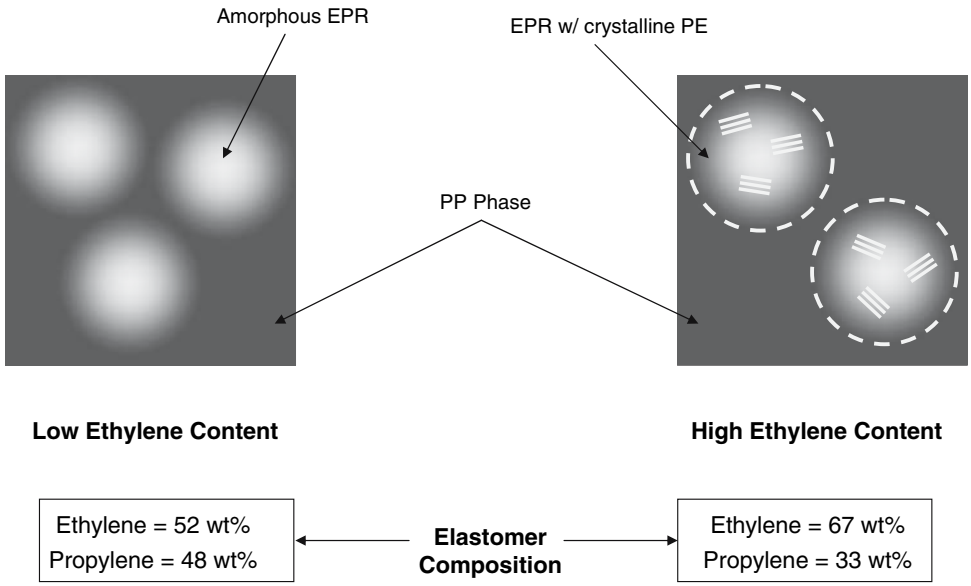

Fig. 2 Schematic illustration of internal morphology of model soft TPO systems. Overall composition is 70 wt.% EPR and 30 wt.% PP

schematic of the resulting internal morphologies that result as a consequence of increasing the ethylene content of EPR.

This morphology alteration was supported by SEM observation. Figure 3 shows micrographs of cross sections of Systems A and B after being subjected to etching with a chromic acid agent. The light gray features in the micrographs represent the EPR phase that has been etched away.

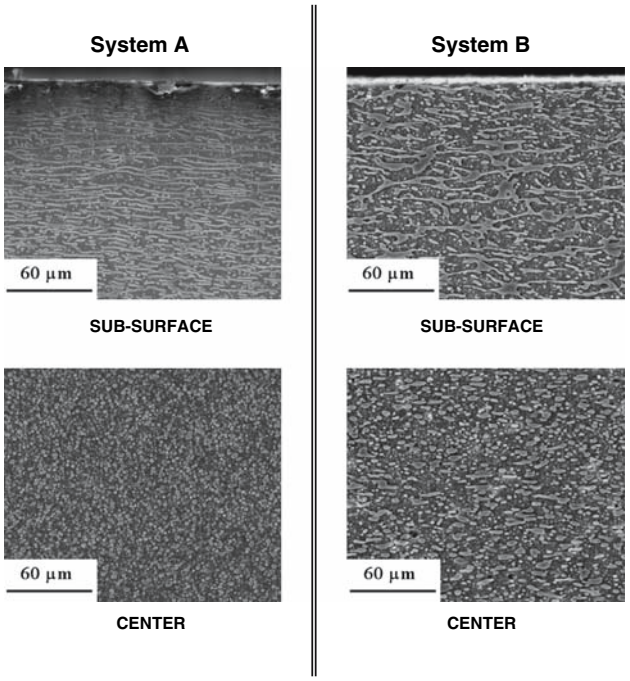

Fig. 3 SEM micrographs of cross sections of model soft TPO systems taken at the sample sub-surface and center. Elastomer phase (light gray color) has been preferentially etched away with a chromic acid agent

Overall, the EPR of System B displays a larger domain size than that of System A. These results suggest that the interaction between the EPR and PP phases is indeed improved in a blend of low-ethylene-content EPR and PP (System A) and results in a more homogeneous blend.

Changing the morphology of the material appears to affect the mechanical properties, as well. Engineering stress–strain curves obtained under various testing rates for the model soft TPOs are shown in Figs. 4 and 5. Apparent tensile strength was taken as the maximum point of the stress–strain curves, as per ASTM D412. Increases in the apparent tensile strength, percent elongation at failure, and Shore-A hardness were observed with an increase in ethylene content of the elastomer (see Figs. 6–8, respectively). These increases can be attributed to the increase in the EPR crystallinity.

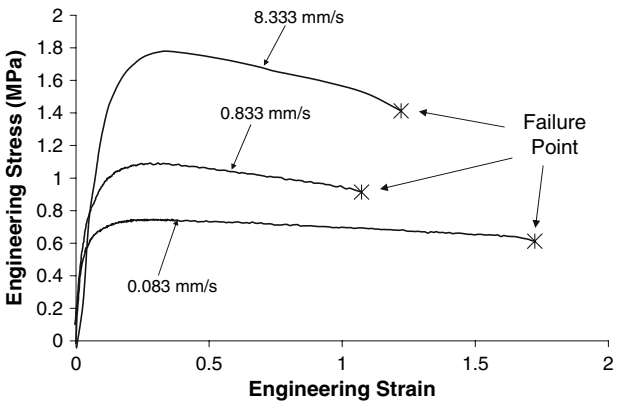

Fig. 4 Engineering stress–strain curves for System A tested at various rates

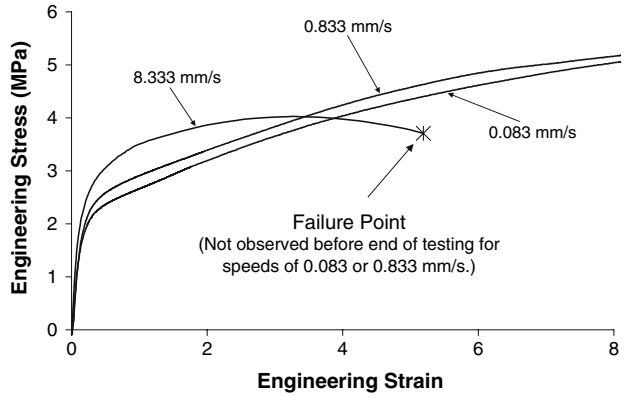

Fig. 5 Engineering stress–strain curves for System B tested at various rates

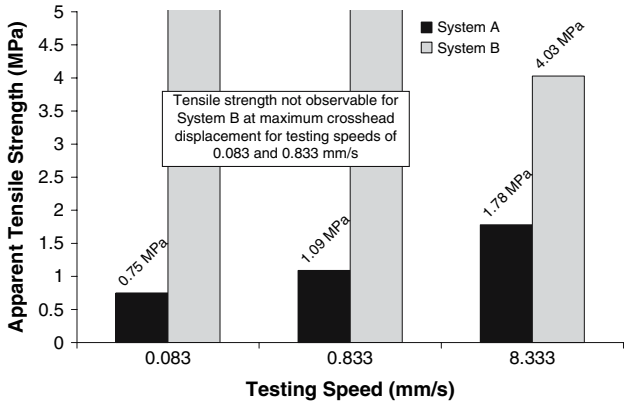

Fig. 6 Apparent tensile strength of model systems

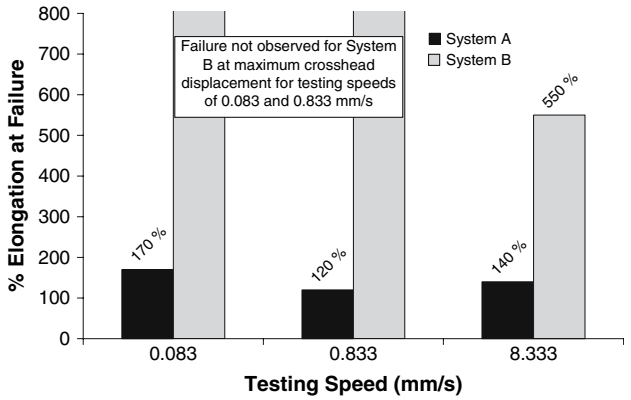

Fig. 7 Elongation at failure point of model systems

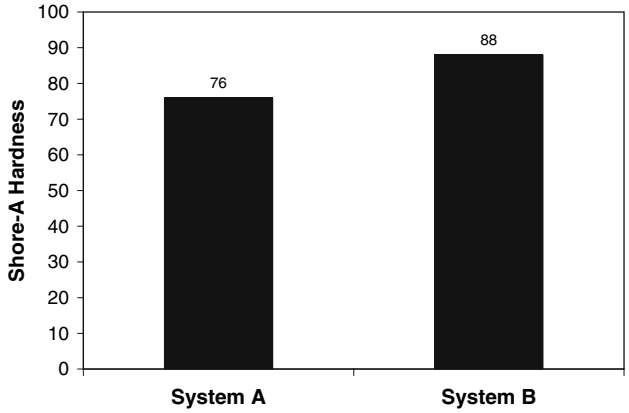

Fig. 8 Shore-A hardness of model systems

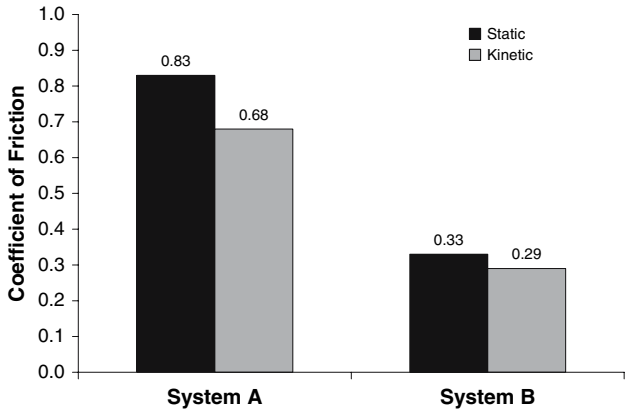

Fig. 9 Static and kinetic coefficients of friction for model systems

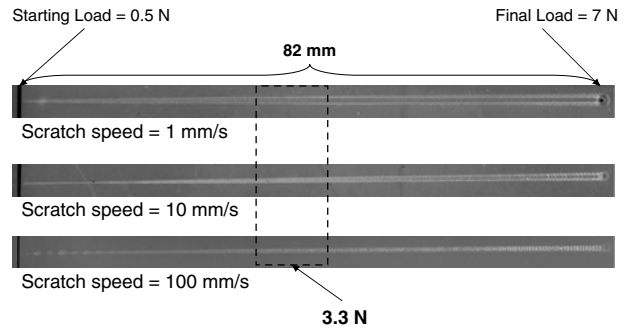

Fig. 10 Images of optically scanned scratched samples of System A. Resolution = 800 dpi. The bounded box indicates the area used in SEM observation (Scratch direction is from left to right)

Figure 9 shows that increasing the ethylene content can lower the static and kinetic coefficient of friction (COF). This is expected since System A is the softer material as evidenced by its lower Shore-A hardness. It is known that soft materials require a higher tangential force to initiate movement due to the higher penetration depth and adhesive force they impart. As COF is defined as the ratio of tangential-to-normal force, an increase in tangential force given by a softer system will give rise to higher values of COF at the same value of normal force, as reflected in Fig. 9.

Figures 10 and 11 seem to show that the ethylene content of the elastomer can affect the scratch visibility, as well. For System B, there are two images shown at each speed. The top image is the original obtained from the PC

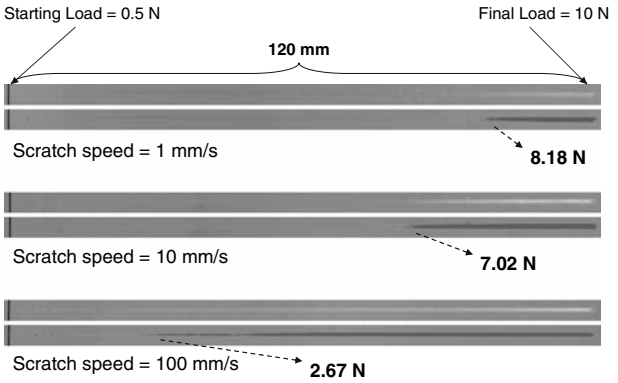

Fig. 11 Images of optically scanned scratched samples (top image for each scratch speed) and corresponding images resulting from processing with imageJ (bottom image for each scratch speed) of System B. Resolution = 800 dpi. Dashed arrows indicate the onset of scratch visibility (Scratch direction is from left to right)

scanner. The bottom images at each testing speed were obtained by applying a grayscale threshold technique with ImageJ digital image analysis software to assess the onset point of scratch visibility. A description of this digital treatment can be found in [15].

Overall, System A shows signs of penetration and ductile drawing, even at the initial portion of scratch loading (Fig. 10). In stark contrast, the scratch damage in System B appears to be subtle, in that it shows no immediately obvious signs of penetration or drawing. Rather, it shows evidence of markedly different scratch damage behavior in the form of stress whitening (Fig. 11). This strong difference in scratch damage appearance is likely related to the differences in morphology, hardness, and tensile behavior, which results from the differences in EPR matrix crystallinity between the two systems.

When viewed at higher resolution with an SEM, the difference in scratch damage features becomes even more evident (Fig. 12). Micrographs for System A were taken for each testing speed at the point corresponding to 3.3 N. At this point, the fish-scale feature was fully developed at a testing speed of 10 mm/s. This provides a fair point of comparison for 1 and 100 mm/s. Micrographs are shown for System B at each testing speed at the location just after scratch visibility occurs at 1 mm/s. At this point, the scratch damage of System B is visible at all three testing speeds.

It has been observed and shown that the formation of fish scale on rigid TPO surfaces during scratching with a spherical indenter is mainly due to ductile drawing, followed by ironing from the indenter tip on the scratch path [25]. Figure 12 shows that System A appears to be quite sensitive to plastic deformation through extensive fish-scale formation. The behavior of System B in Fig. 12 suggests that it possesses a high amount of viscoelastic recovery when compared to System A, possibly due to the

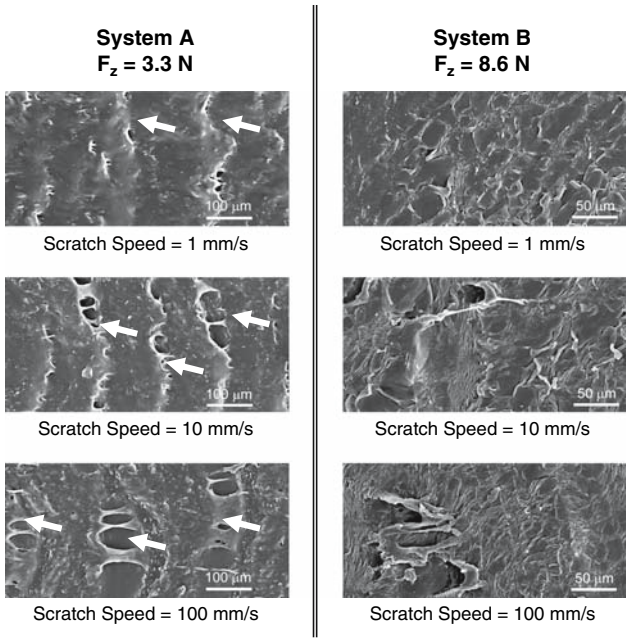

Fig. 12 High-magnification SEM micrographs of scratch damage observed in model soft TPO systems

presence of crystalline PE that leads to the formation of physical cross-links. As a result, System B does not show signs of extensive fish scaling. Instead, it shows signs of small-scale void formation, likely resulting from EPR/PP debonding.

It is noted that a small amount of plastic deformation in the form of drawing occurs in System B (Fig. 12). However, since the viscoelastic recovery of System B is so great compared to that of System A, void formation is the governing scratch damage mechanism. This suggests that the bonding strength in the crystalline EPR/PP blend is weaker than that of the amorphous EPR/PP blend. From these results, under these scratch testing conditions, it can be said that System A yields at a lower load while System B yields at a higher load and exhibits pronounced viscoelastic recovery due to the presence of the crystalline PE phase which serves as a physical crosslinker. The above finding is in good agreement with the FEM modeling results of Jiang et al. [18].

In an attempt to explain why crystallinity could play such an important role in the scratch damage, consider the schematic engineering stress-strain curves for different elastomers given in Fig. 13. The three curves represent typical tensile behavior observed for three materials: a vulcanized rubber and the two types of soft TPOs in this study. The behavior of a hyper-elastic material with chemical cross-linking (i.e., vulcanized rubber) follows the neo-Hookean or Mooney-Rivlin model (Fig. 13(a)). Under uniaxial tension, the material first experiences large-scale deformation where the chains between cross-links begin to

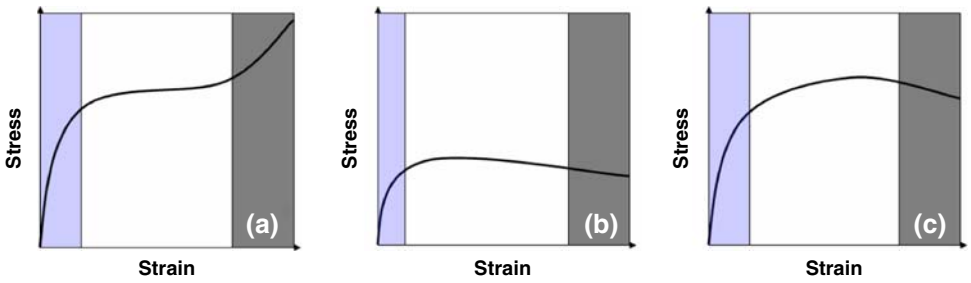

Fig. 13 Schematic engineering stress–strain curves for different elastic materials: (**a**) Chemically cross-linked rubber, (**b**) EPR-rich TPO containing low-ethylene content EPR (System A), and (**c**) EPR-rich TPO containing high-ethylene content EPR (System B)

slide past one another (light-gray region). After the chains have reached their maximum deformation limit, the curve will plateau (white region) as the strain increases while the molecular network re-organizes itself. This is followed by increase in stress after the molecular network has begun to align and reach its deformation limit (dark-gray region). The final step is ultimate failure of the material via chain scission.

The behavior of the soft TPOs of this study appears to follow the neo-Hookean behavior within the first region (Figs. 13(b and c)). After this, there is a deviation which is likely caused by the nature of their individual matrix characteristics. Vulcanized rubbers have covalent, chemical cross-links that reinforce the material, which can account for the increase in stress in the third region of the engineering stress–strain curve. The TPOs of this study do not possess chemical cross-links. However, the crystalline portions within the EPR of System B serve to function as physical cross-links. This allows the material to behave like a rubber within the second region, showing signs of significant elastic recovery. In the third region, the crystalline portions begin to disintegrate, resulting in the decrease in stress seen in Fig. 13(c). System A has no cross-links of any kind and simply yields after the first region.

Effect of scratch testing rate

The rate-dependent tensile behavior of the soft TPOs suggests that the scratch behavior might also display rate dependency. Figures 10 and 11 confirm that both soft TPO systems do in fact possess strong rate-dependent scratch behavior. When compared to the scratch behavior of rigid TPOs, soft TPOs are significantly more rate-dependent [48]. As a consequence, care should be taken when evaluation of scratch resistance is carried out on soft TPOs.

When System A is viewed on the large scale, obvious testing rate dependence can be observed (see Fig. 10). As the scratch testing rate is increased, the damage appears to evolve from penetrative ploughing to surface drawing. This implies that a soft material will appear to be more rigid at high testing rates, as would be expected for viscoelastic materials.

The SEM micrographs of the damage features shown in Fig. 12 serve to show the impact of the testing rate on the scratch damage feature. These micrographs show that increasing the scratch testing rate, while keeping the applied normal load constant, seems to change the appearance of the fish-scale feature. As the testing rate is increased, the periodic fish-scale feature (indicated with white arrows) shifts from an almost-smooth feature to a series of what appear to be surface voids connected by fibrils.

The earlier claim that the damage in System A appears to become less penetrative at higher scratch testing speeds is supported by the scratch depth profile curves shown in Fig. 14. System A does indeed undergo less penetration when scratched at higher speeds. This result along with the subtle micro-voiding just mentioned supports the claim that a soft, viscoelastic material will appear more rigid and possibly stronger at high testing speeds (Fig. 4).

Conversely, the rate dependence of System B is not as evident in the scratch damage feature as it is in the critical load where scratch visibility begins (see Fig. 11). The values of the critical load (F_c) calculated using Eq. 1 at each testing rate for which this occurs are displayed in chart form in Fig. 15. Viewing these values alongside those for apparent tensile strength shown in Fig. 6 shows that increasing the testing speed yields a great drop in the apparent tensile strength and the critical load for scratch visibility.

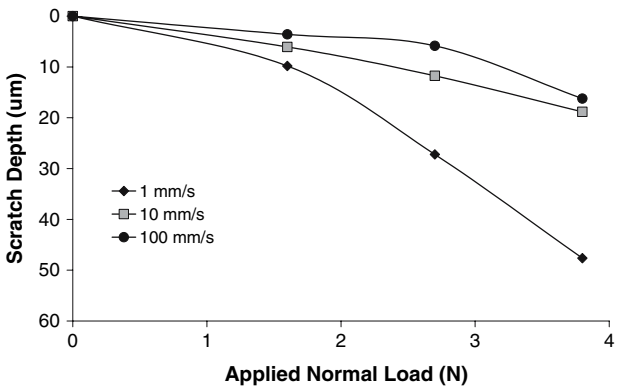

Fig. 14 Scratch depth as a function of applied normal load for System A at various scratch speeds

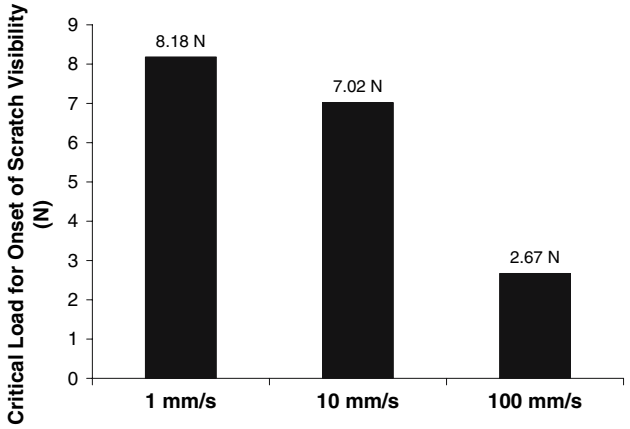

Fig. 15 Critical load for onset of scratch visibility for System B

As the scratch testing rate increases, the damage appearance of System B does not appear to change substantially from a damage feature standpoint (see Fig. 11). However, viewing the damage at a higher magnification where all systems display scratch visibility, shows that there are differences that occur as a result of changing the testing speed (see Fig. 12). The dominant failure mechanism for System B is micro-voiding likely resulting from weak EPR/PP bonding. These micro-voids scatter incident light and lead to scratch visibility.

From Fig. 6, it can be seen that System B experiences a drop in apparent tensile strength with increasing scratch speed. This seems to tie in with the appearance of the scratch damage shown in Fig. 12. As the scratch speed increases, the "islands" formed from the debonding process get smaller. Additionally, there appears to be a small amount of drawing of the material. This behavior is in direct contrast to that of System A which exhibits increasing apparent tensile strength and increasingly more rigid behavior. This implies that the presence of crystalline domains within the EPR could lead to an entirely different scratch-induced damage feature, which may render different strategies for improving scratch resistance of soft TPOs.

The present work seems to suggest that EPR ethylene content and testing speed imparts a significant effect on the scratch behavior of "soft-touch" EPR-rich TPOs. Compared to their more rigid counterparts (i.e., TPOs containing 70 wt.% PP and 30 wt.% EPR), soft TPOs are more delicate and will be easily scratched in low-load scenarios. It is possible, however, to improve the scratch resistance of the material itself. Increasing the ethylene content appears to increase both the Shore-A hardness and the relative magnitude of apparent tensile strength, which is attributed to the presence of crystalline PE segments within the EPR, as shown by DSC. The higher magnitude of apparent tensile strength in System B implies higher elastic recovery due to the physical cross-linking of PE crystals. Thus, resistance to penetrative scratching is improved.

Worth noting is that increasing the scratch testing speed exhibits an improvement in scratch resistance for soft TPOs with amorphous EPR. On the other hand, a soft TPO with crystallite-containing EPR will exhibit weakened scratch resistance through scratch visibility with increasing scratch speed. Through a parametric study using finite element analysis of the polymer scratch process, Jiang et al. found that a significant improvement in scratch behavior comes from adjusting the properties of yield strength and COF [18]. The yield strength is tied to the polymer's ability to undergo plastic deformation (drawing/fish-scale, plouing, cutting, and pile-up), while the COF is related to the amount of force the tip imparts as it scratches the surface. This means that even though "soft-touch" TPOs are inherently more delicate than rigid TPOs, their mechanical properties can be improved to give the best scratch performance.

This study makes an effort to tie the scratch behavior of the soft TPO systems to their tensile behavior. In reality, the scratch phenomenon is significantly more complex and requires careful analysis regarding the applied stresses. The stress field involved in an increasing load scratch test not only has elements of tensile behavior, but also simultaneously contains compressive and shear components, as well. Therefore, future efforts will be made to correlate the scratch behavior of polymers with mechanical properties in a multi-axial stress nature.

In summary, the scratch resistance of EPR-rich soft TPOs can be optimized by taking advantage of the fact that their morphology can be manipulated to give optimal apparent tensile yield stress and/or strength, depending on the scratch damage mechanisms observed. Further steps that could improve scratch resistance are reduction in domain size, better bonding between the EPR and PP, and cross-linking of the elastomer to give a stronger material with better elastic and viscoelastic recovery.

Conclusions

Soft TPO materials consisting of a 70/30 wt.% blend of EPR/PP were subjected to a standardized scratch test to study the effect of scratch testing rate. The effect of EPR ethylene content was investigated by setting the ethylene content to 52 wt.% (System A) and to 67 wt.% (System B). Higher ethylene content in EPR appears to allow the PE segments to crystallize and form physical cross-links, resulting in a harder, more elastic recoverable material. This, in turn, leads to weak interfacial bonding between the EPR and PP in System B. As a result, the damage in

System A shows up as penetration and surface drawing (or "fish-scale") whereas the dominant damage mechanism for System B is stress whitening caused by micro-voids. With regard to increased scratch rate, the scratch depth of System A decreases as the scratch rate increases. The more rigid System B shows earlier onset of visibility associated with micro-voiding as the scratch speed increases. The rate-dependent behavior of both Systems A and B implies that soft TPOs will experience a significant amount of embrittlement and behave more rigidly at high mechanical testing rates.

Acknowledgements The authors would like to recognize the financial support of the Texas A&M University Scratch Behavior of Polymers Consortium (http://www.ptc.tamu.edu). Thanks also go to Sumitomo Chemical for supplying material and evaluation of property data. Microscopy work at Texas A&M University was conducted in the Microscopy and Imaging Center.

References

1. Chang SH, Dong JI, Sung CK (1986) J App Poly Sci 32:6281
2. Choudhary V, Varma HS, Varma IK (1991) Polymer 32:2541
3. D'Orazio L, Cecchin G (2001) Polymer 42:2675
4. D'Orazio L, Mancarella C, Martuscelli E, Cecchin G, Corrieri R (1999) Polymer 40:2745
5. Katbab AA, Nazockdast H, Bazgir S (2000) J App Poly Sci 75:1127
6. Kim BK, Do IH (1996) J App Poly Sci 61:439
7. Cai HJ, Luo XL, Chen XX, Ma DZ, Wang JM, Tan HS (1999) J App Poly Sci 71:103
8. Shariatpanahi H, Nazokdast H, Dabir B, Sadaghiani K, Hemmati M (2002) J App Poly Sci 86:3148
9. Tasdemir M, Topsakalolu M (2007) J App Poly Sci 104:3895
10. Varghese S, Alex R, Kuriakose B (2004) J App Poly Sci 92:2063
11. Da Silva ALN, Coutinho FMB (1996) Poly Test 15:45
12. Fu ZS, Fan ZQ, Zhang YQ, Feng LX (2003) Euro Poly J 39:795
13. Goharpey F, Nazockdast H, Katbab AA (2005) Poly Eng Sci 45:84
14. Pires M, Mauler RS, Liberman SA (2004) J App Poly Sci 92:2155
15. Browning R, Lim GT, Moyse A, Sun LY, Sue HJ (2006) Poly Eng Sci 46:601
16. Browning RL, Lim GT, Moyse A, Sue HJ, Chen H, Earls JD (2006) Surf Coat Tech 201:2970
17. Chu J, Xiang C, Sue HJ, Hollis RD (2000) Poly Eng Sci 40:944
18. Jiang H, Lim G-T, Reddy J, Whitcomb J, H-J Sue (2007) J Poly Sci B Poly Phys 45:1435
19. Urban MW (2005) Stimuli-responsive polymeric films and coatings, ACS Symposium Series #912. Oxford University Press and American Chemical Society, Washington, DC, p 166
20. Lim GT, Wong MH, Reddy JN, Sue HJ (2005) J Coat Tech Res 2:361
21. Lu J, Wei GX, Sue HJ, Chu J (2000) J App Poly Sci 76:311
22. Wong JSS, Sue HJ, Zeng KY, Li RKY, Mai YW (2004) Acta Mat 52:431
23. Wong M, Lim GT, Moyse A, Reddy JN, Sue HJ (2004) Wear 256:1214
24. Wong M, Moyse A, Lee F, Sue HJ (2004) J Mat Sci 39:3293
25. Xiang C, Sue HJ (2001) J App Poly Sci 82:3201
26. Xiang C, Sue HJ, Chu J, Coleman B (2001) J Poly Sci B Poly Phys 39:47
27. Xiang C, Sue HJ, Chu J, Masuda K (2001) Poly Eng Sci 41:23
28. Bermudez MD, Brostow W, Carrion-Vilches FJ, Cervantes JJ, Damarla G, Perez JM (2005) E-Polymers No. 003
29. Briscoe BJ, Biswas SK, Sinha SK, Panesar SS (1993) Tribol Int 26:183
30. Briscoe BJ, Evans PD, Pelillo E, Sinha SK (1996) Wear 200:137
31. Bucaille JL, Felder E (2002) Philos Mag A 82:2003
32. Bucaille JL, Gauthier C, Felder E, Schirrer R (2006) Wear 260:803
33. Dasari A, Kolluru S, Rohrmann J, Misra RDK (2003) Mater Sci Tech Lond 19:1289
34. Dasari A, Perkins RS, Rohrmann J, Misra RDK (2003) Mater Sci Tech Lond 19:1279
35. Dasari A, Rohrmann J, Misra RDK (2003) Mater Sci Tech Lond 19:1458
36. Jardret V, Morel P (2003) Prog Org Coat 48:322
37. Lin L, Blackman GS, Matheson RR (2000) Prog Org Coat 40:85
38. Lin L, Blackman GS, Matheson RR (2001) Mat Sci Eng A Struct 317:163
39. Ryntz RA, Britz D (2002) J Coat Tech 74:77
40. Shen W (2006) JCT Coat Tech 3:44
41. Shen W (2006) JCT Coat Tech 3:54
42. Shen W, Jiang B, Scholten A, Schwenke R, Mi L, Seal C, Wang P (2004) Tribol Lett 17:637
43. ASTM D7027-05 (2005) Standard test method for evaluation of scratch resistance of polymeric coatings and plastics using an instrumented scratch machine. ASTM International
44. Pizzoli M, Righetti MC, Vitali M, Ferrari P (1998) Polymer 39:1445
45. Da Silva ALN, Rocha MCG, Lopes L, Chagas BS, Coutinho FMB (2001) J App Poly Sci 81:3530
46. Yamaguchi M, Miyata H, Nitta KH (1996) J App Poly Sci 62:87
47. Pukanszky B, Tudos F, Kallo A, Bodor G (1989) Polymer 30:1399
48. Wong M (2004) Test method development for evaluation of scratch behavior of polymers. MS Thesis, Texas A&M University